An in vivo active 1,2,5-oxadiazole Pt(II) complex: a promising anticancer agent endowed with STAT3 inhibitory properties

Federica Porta,[a±] Giorgio Facchetti,[a±] Nicola Ferri,[b] Arianna Gelain,[a*] Fiorella Meneghetti,[a] Stefania Villa,[a] Daniela Barlocco,[a] Daniela Masciocchi,[a] Akira Asai,[c] Nao Miyoshi,[c] Silvia Marchianò,[d] Byoung-Mog Kwon,[e] Yena Jin, [e] Valentina Gandin,[b] Cristina Marzano,[b] Isabella Rimoldi.[a*]*

[a] Dipartimento di Scienze Farmaceutiche, Università degli Studi di Milano, Via L. Mangiagalli 25, 20133 Milano, Italy

[b] Dipartimento di Scienze del Farmaco, Università degli Studi di Padova, Via Marzolo 5, 35131, Padova, Italy

[c] Center for Drug Discovery, Graduate School of Pharmaceutical Sciences, University of Shizuoka, 52-1 Yada, Suruga-ku, Shizuoka, 422-8526, Japan

[d] Dipartimento di Scienze Farmacologiche e Biomolecolari, Università degli Studi di Milano, Via Balzaretti 9, 20133 Milano, Italy

[e] Korea Research Institute of Bioscience and Biotechnology, University of Science and Technology, 125 Gwahakro Yoosunggu, Daejeon 34141

KEYWORDS: DNA-interaction, cytotoxic activity, platinum diamine complex, antitumor agents, protein–protein interactions.

ABSTRACT. New Pt(II) complexes (**Pt-1-3**) bearing 1,2,5-oxadiazole ligands (**1-3**) were synthesized, characterized and evaluated for their ability to disrupt STAT3 dimerization. Ligand **3** · **HCl** showed cytotoxic effects on HCT-116 cells (IC_{50} = 95.2 µM) and a selective ability to interact with STAT3 (IC_{50} = 8.2 µM) *versus* STAT1 (IC_{50}> 30 µM). Its corresponding platinum complex **Pt-3** exhibited an increased cytotoxicity (IC_{50} = 18.4 µM) and a stronger interaction with STAT3 (IC_{50} = 1.4 µM), leading to inhibition of its signaling pathway. **Pt-3** was also evaluated in cell-based assays for its action on p53 expression and on STAT3 phosphorylation. In syngeneic murine Lewis lung carcinoma (LLC) implanted in C57BL/6 mice, **Pt-3** showed a higher antitumor activity with fewer side effects than cisplatin.

1. INTRODUCTION

The development of cisplatin and other cytotoxic metal complexes have contributed to tremendous advances in the field of chemotherapy based on metallorganic entities over the past few decades.[1-3] The Food and Drug Administration (FDA)-approved Pt-based anticancer drugs cisplatin, carboplatin and oxaliplatin are still among the most effective drugs used for the treatment of solid cancers.[4-6] These Pt-based anticancer agents typically form bifunctional intra- and interstrand DNA cross-links through covalent bonds with purine nucleobases, inhibiting transcription and resulting in cell-death. Unfortunately, the strong side effects and the increasing resistance are limitations to their use, thus evoking the need for new Pt-based chemotherapeutics.[7-10]

Literature data highlighted that cisplatin, besides interacting with DNA, was able to modulate mitogen-activated protein kinase (MAPK) family and the phosphoinositide 3 (PI-3)-kinase/Akt pathway.[11, 12] Moreover, many platinum complexes displayed an effective inhibition of signal transducer and activator of transcription 3 (STAT3) cascade,[13, 14] leading to significant clinical benefits. Indeed STAT3 is constitutively activated in a variety of human cancers, including solid tumors, such as breast, prostate and cervical cancers, as well as many leukemias and lymphomas.[15]

In this regard, kinetically liable Pt(IV) complexes inducing tumor regression in mouse colon cancer model, were established to inhibit STAT3 activity in living cells through an irreversible interaction with the STAT3 DNA-binding domains.[13] The involvement of STAT3 activated cellular responses in cisplatin resistant tumors was highlighted by the ability of Stattic, an effective STAT3 inhibitor, to restore the sensitivity to Pt-based drugs both *in vitro* and *in vivo*.[16, 17] Complexes endowed with these dual-targeting features could lead to enhanced therapeutic benefits, as we expect tumor cell apoptosis with minimal side effects.[18]

The effect on STAT3 signaling cascade has been often related to platinum complexes[13] and small molecules (Stattic and S3I-201)[19] capability to interact with thiol moiety of cysteines, leading to STAT3 dimerization disruption. Moreover, the disulphide bond-mediated STAT3-dimer formation might be due to the presence of several cysteine residues or vicinal polar residue serving to activate the target cysteine

while analogous aggregates through disulphide bond formation haven't been observed related to STAT1.[20]

Among the molecules disclosed as potential antitumor agents, oxadiazoles have received considerable attention in recent years because of their interesting activity.[21, 22] In this respect, the oxadiazole ring emerged as a key molecular feature for STAT3 inhibition, amongst others, the 1,3,4-oxadiazole characterizes STX-0119,[23, 24] while the 1,2,5-oxadiazole isomer is present in AVS-0288,[25] both known as potent STAT3 inhibitors. All these findings supported our ongoing research focusing on the design of new platinum complexes possibly able to simultaneously interact with DNA and to interrupt STAT3 signaling.[18] Taking advantage of our experience in the chemistry and biology of the oxadiazole ring[26-28] and of platinum compounds,[29, 30] we planned the synthesis of 3-aminomethyl-1,2,5-oxadiazole derivatives as ligands in Pt(II) complexes (**Figure 1**).[31]

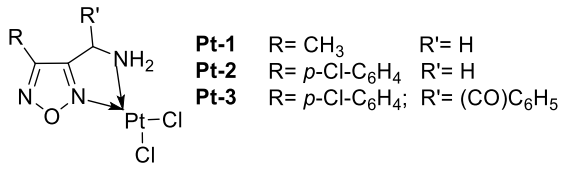

Figure 1. New Pt(II) complexes.

2. RESULTS AND DISCUSSION

In this study, we designed 1,2,5-oxadiazole derivatives and their Pt(II) complexes with the aim to obtain a dual mechanism of action: interfering with DNA replication and inhibiting STAT3 signaling pathway. We devised an aminomethyl moiety as the pivotal feature to be introduced in the 3 position of the oxadiazole ring in order to realize a planar-coordinated Pt(II) drug. Therefore, since our previous research on 1,2,5-oxadiazole derivatives[27] allowed us to identify *p*-chlorophenyl and benzoyl as useful moieties for STAT3 interaction, starting from the commercially available 3-aminomethyl-4-methyl-1,2,5-oxadiazole (**1**), compound **2** (bearing a *p*-chlorophenyl system at 4-position of the heterocycle) and compound **3** (presenting also a benzoyl group on the aminomethyl chain) were designed and synthesized. Hence, compounds **1**, **2 · HCl** and **3 · HCl** were used in coordination with Pt(II) centre. Both ligands and metal complexes (**Figure 2**) underwent biological evaluation.

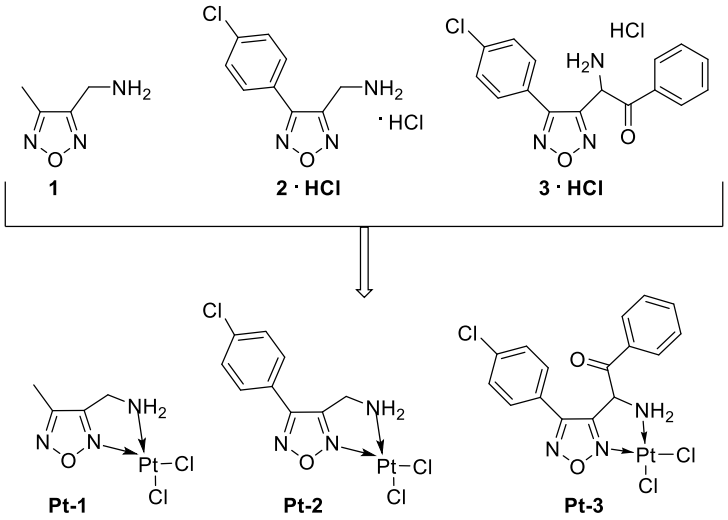

Figure 2. Ligands and their corresponding Pt(II) complexes.

a. Synthetic Strategy. The synthesis of compounds **2**, **3**, **Pt-1**, **Pt-2** and **Pt-3** are shown in **Schemes 1-3.**

Intermediate **4** was synthesized starting from the commercially available *p*-chlorocinnamic acid, according to the literature.[32] Azide **5** was prepared by a one pot reaction[33] in presence of NaN_3 and Ph_3P in CCl_4/DMF, and converted to the corresponding amine **2** by catalytic hydrogenation (**Scheme 1**). The final product was isolated as hydrochloride salt (**2** · **HCl**).

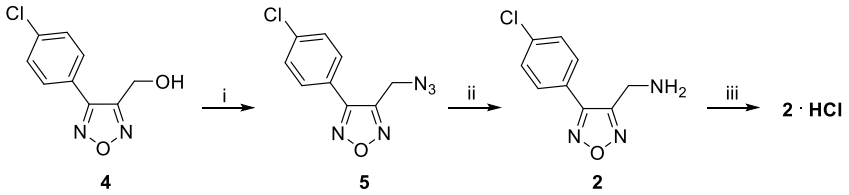

Scheme 1. Reagents and conditions: *i)* NaN_3, Ph_3P, CCl_4/DMF (1:4), 90°C, 5 h; *ii)* Pd/C, H_2, MeOH, 20 atm, 4 h; *iii)* 2 M HCl in Et_2O.

The synthesis of compound **3** (**Scheme 2**) started from the commercially available *p*-chloropropiophenone which was treated with *tert*-butyl nitrite and chlorotrimethylsilane to obtain the correspondent *α*-ketooxime **6**. This was converted to the *bis*-oxime **7**, in presence of hydroxylamine hydrochloride and sodium hydroxide,[34] and then cyclized with potassium hydroxide and cesium carbonate at high temperature to give intermediate **8**. Treatment with *n*-butyl lithium and methyl benzoate gave ketone **9** which underwent an *α*-oximation with *tert*-butyl nitrite and chlorotrimethylsilane. The reduction of compound **10** with zinc in trifluoroacetic acid led to product **3**, purified as hydrochloride salt**.**

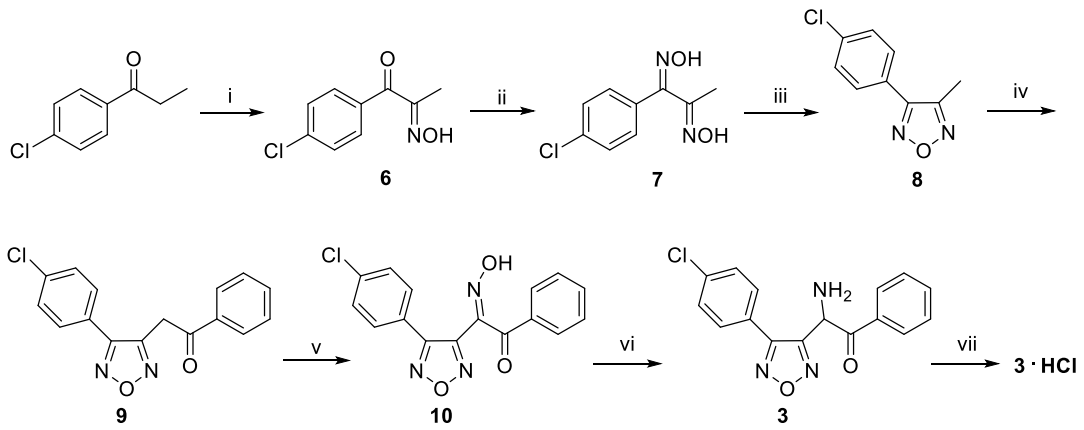

Scheme 2. Reagents and conditions *i) t*-BuONO, TMSCl, dry THF/DCM, -20°C to rt, 12 h; *ii)* $NH_2OH{\cdot}HCl$, NaOH, H_2O, reflux, 3 h; *iii)* KOH, Cs_2CO_3, ethylen glycol, 160°C, 1.5 h; *iv)* 2.5 M *n*-BuLi in hexane, methyl benzoate, dry THF, -55°C for 1 h, then rt for 12 h; *v) t*-BuONO, TMSCl, dry THF, -20°C to rt, 12 h; *vi)* Zn, TFA, rt, 40 min; *vi)* 2 M HCl in Et_2O.

A classical methodology was employed for the preparation of the corresponding Pt(II) complexes.[35] Accordingly, **1**, **2** · **HCl** and **3** · **HCl** were treated with K_2PtCl_4 in water in presence of 4 M HCl affording the target compounds **Pt-1**, **Pt-2** and **Pt-3** (**Scheme 3**).

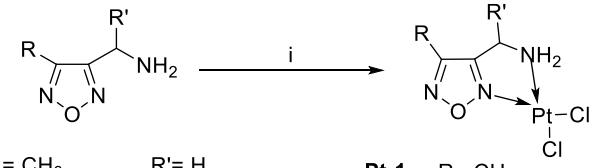

1	R= CH_3	R'= H
2 · HCl	R= p-Cl-C_6H_4	R'= H
3 · HCl	R= p-Cl-C_6H_4	R'= $(CO)C_6H_5$

Pt-1	R= CH_3	R'= H
Pt-2	R= p-Cl-C_6H_4	R'= H
Pt-3	R= p-Cl-C_6H_4	R'= $(CO)C_6H_5$

Scheme 3. Reagents and conditions: *i)* K_2PtCl_4, 4 M HCl, H_2O, reflux, 2 h.

2.2 Characterization. The identity and purity of all synthesized compounds and their Pt(II) complexes were ascertained by ^{1}H NMR, ^{195}Pt NMR, ESI-MS, ~~or~~ elemental analysis and IR (see spectra in SI). The observed chemical shifts (around -2070 ppm) for ^{195}Pt NMR spectra are in the range expected for a Pt(II) core with a N_2Cl_2 coordination environment,[36]. In the infrared spectra, the strong absorption around 3200-3100 cm^{-1} corresponding to the N-H stretching vibration resulted significantly red shifted in comparison to the corresponding free ligands. The coordination geometry was confirmed by single-crystal X-ray diffraction on the complex **Pt-1**. The ORTEP diagram of **Pt-1** is shown in **Figure 3** with selected bond distances and angles. This compound crystallized with two independent molecules in the asymmetric unit, which are almost planar and parallely oriented.

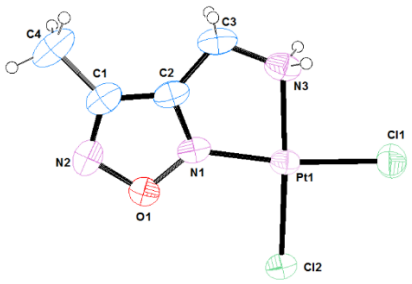

Figure 3: ORTEP[37] view of one of the two molecules present in the asymmetric unit of **Pt-1**, showing the arbitrary atom labeling scheme. Ellipsoids are drawn at 40% probability level and H atoms are shown as spheres of arbitrary radius. Selected averaged bond distances (Å): Pt-N1, 1.956(1); Pt-N3, 2.046(1); Pt-Cl1, 2.274(1); Pt-Cl2, 2.294(1); N1-C2, 1.291(1); N3-C3, 1.497(1). Angles (°): N1-Pt-N3, 80.8(1); N3-Pt-Cl1, 90.7(1); Cl1-Pt-Cl2, 91.6(1); Cl2-Pt-N1, 96.8(1); C2-N1-Pt, 119.9(1); C3-N3-Pt, 112.2(1); C2-C3-N3, 110.5(1).

The complex **Pt-1** crystallized with two independent molecules in the asymmetric unit with very similar configurations, which are almost planar and parallel oriented. The ORTEP diagram of one molecule is shown in **Figure 3**, with selected bond distances and angles.

The determined lengths and angles values are in agreement with the literature for similar Pt(II) complexes.[38] The Pt(II) atom is coordinated by N atoms of the bidentate ligand and Cl atoms. The coordination environment around the central Pt(II) in both molecules are slightly distorted from an ideal square planar configuration, and the chlorine

atoms are *cis* to each other. The angles around Pt atom are close to the expected 90° and 180°. The mean deviation of the PtNNClCl coordination plane is ca. 0.030(6) Å (N1) and the methyl groups lie almost in the same plane of the oxadiazole ring.

In the unit cell, two non-equivalent dimers head-to-tail are formed by π–π interactions between individual complexes. These latter are stacked forming molecular layers, parallel to the *ab* plane, where consecutive molecules interact through Pt···Pt contacts at 3.612 and 3.3364 Å,[39] developing chains along the *c* axis[40] also consolidated by N-H···Cl type interactions.

2.3 Aqueous stability and lipophilicity. The aqueous stability for Pt(II) complexes were performed using 0.9 % *w/v* NaCl solution in DMF by monitoring UV-vis spectra at their respective λ_{max} during a period of 48 h. Each compound was first dissolved in DMF and then diluted with physiological solution to 100 μM final concentration (1% *v/v* DMF). **Pt-1**, **Pt-2** and **Pt-3** demonstrated good stability in physiological solution with negligible variation of their UV peak profile after 48 h. (see spectra in SI)

The values of log P_{ow} were determined using RP-HPLC technique.[41-43] The lipophilicity increased along the series (-0.123 and 2.28 for **1** and **2** · **HCl**, respectively), reaching the maximum value of 1.09 and 3.01 with **3** · **HCl**. The same trend characterized Pt(II) compounds (-0.773, 2.00 and 2.99 for **Pt-1**, **Pt-2** and **Pt-3** respectively) still satisfying the Lipinski's lipophilicity criterion for druglikeness. Ligand **3** showed a keto-enolic equilibrium responsible for the racemization at the chiral centre,[44, 45] as confirmed by the two values of log P_{ow}. Its tautomerism was evaluated at different pH conditions by RP-HPLC (**Figure 4**): the peaks showed the different ratio between the ketone and the enol species confirming the stability of the compound in all cases.

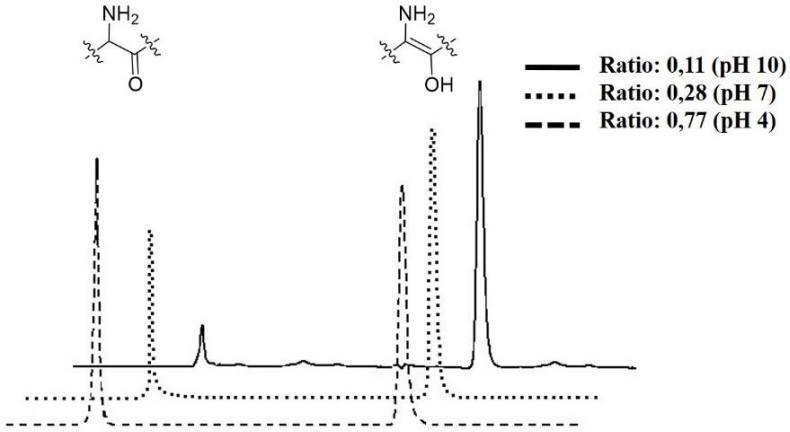

Figure 4: pH dependent ligand **3** enolization ratio (keto /enol) using RP-HPLC Partisil C-18 ODS.

2.4 *In vitro* biological evaluation. The ligands and their corresponding complexes were tested by MTT assay for cytotoxic activity and AlphaScreen-based assay to evaluate the effect on STAT3 dimerization.

MTT assay on HCT-116. The cytotoxic effect of the new ligands and their corresponding Pt(II) complexes was initially assessed in cultured colorectal cancer cells HCT-116. The cell viability was estimated by MTT assay after 48 h incubation with increasing concentrations (10 ÷ 150 μM) of the compounds. As reported in **Table 1**, the ligands generally expressed a negligible (**1** and **2** · **HCl**) or weak (**3** · **HCl**) cytotoxic activity (IC_{50} = 95.2 μM). However, the coordination to the platinum centre resulted in an increased cytotoxicity with respect to the free ligand. In particular, **Pt-3** displayed the lowest IC_{50} value (18.4 μM), being about 5 times more effective than the uncoordinated **3** · **HCl** ligand.

AphaScreen-based assay. This test is an *in vitro* competitive binding test used to identify compounds able to inhibit the binding of SH2-containing proteins to their correspondent phosphopeptides (5-carboxyfluorescein (FITC)-GpYLPQTV for STAT3 and FITC-GpYDKPHVL for STAT1). Compounds characterized by an interesting affinity were also investigated for their selectivity *versus* STAT1 having a high degree of sequence homology to STAT3 (78%) but an opposite physiological role.[46, 47] Ligands **1** and **2** · **HCl** did not disrupt STAT3 dimerization whereas their corresponding Pt(II) complexes **Pt-1** and **Pt-2**, possessed high inhibitory properties. On the other hand, ligand **3** · **HCl** was shown to selectively interfere with STAT3 (IC_{50} = 8.2 ± 0.1 μM) over STAT1 (IC_{50} value >30 μM); also its coordination to the Pt(II) center, similarly to ligands **1** and **2**,

improved STAT3 inhibitory activity (IC_{50} = 1.4 ± 0.1 μM) but reduced selectivity *versus* STAT1 (IC_{50} 5.9 ± 0.4 μM). (**Table 1**).

Table 1. Biological properties of the reference (Stattic) and of the oxadiazole derivatives.

Compound	MTT assay on HCT116[a] (IC_{50}, μM)	AlphaScreen[b] (IC_{50}, μM)	
		STAT3	STAT1
Stattic	N.E.	15	＞30
1	N.E.	＞30	N.T.
Pt-1	122.9±12.3	0.4 ± 0.04	1.2 ± 0.1
2 · HCl	N.E.	＞30	N.T.
Pt-2	150±16.9	0.3 ± 0.01	1.9 ± 0.1
3 · HCl	95.2±4.41	8.2 ± 0.1	＞30
Pt-3	18.4±6.9	1.4 ± 0.1	5.9 ± 0.4

[a] IC_{50} values measured by MTT assay on HCT-116 cell lines. N.E.: not effective. [b] The ability to disrupt the binding of STATs to the cognate pTyr–peptide (5-carboxyfluorescein (FITC)-GpYLPQTV for STAT3 and FITC-GpYDKPHVL for STAT1) is expressed as IC_{50}. N.T.: not tested.

2.5 *In vivo* tumor growth inhibition. In the light of MTT assay results, the *in vivo* antitumor activity of **Pt-3** and its uncoordinated ligand was evaluated in a model of solid tumor, the syngeneic murine Lewis lung carcinoma (LLC) implanted i.m. in C57BL/6 mice.

Tumor growth inhibition induced by **Pt-3** was compared with that promoted by the reference metallo-drug, cisplatin. From day 7 after tumor inoculation, when tumors became visible, tumor-bearing mice received daily i.p. doses of **Pt-3** (30 $mg \cdot kg^{-1}$), **3 · HCl** (75 $mg \cdot kg^{-1}$) or cisplatin (1.5 $mg \cdot kg^{-1}$). Cisplatin treatment schedule was selected according to standard protocols designed to optimize its efficacy and minimize the occurrence of adverse events.[48] For the assessment of the adverse side effects,

changes in the body weights of tumor-bearing mice were monitored at day 1 and every two days from day 7 to day 15 (**Figure 5**).

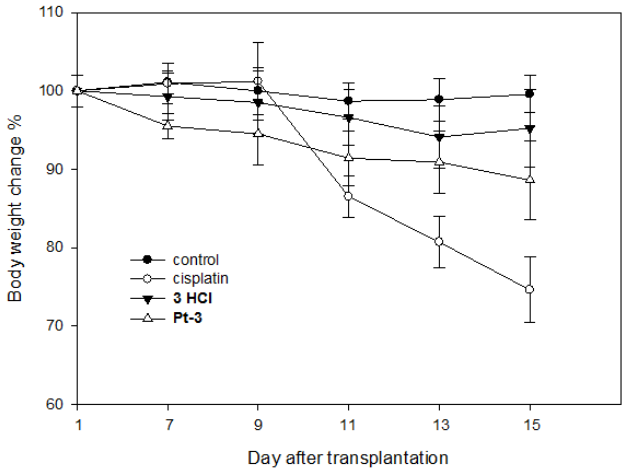

Figure 5. Body weight changes. The body weight changes of LLC-bearing C57BL mice treated with vehicle or tested compounds. Body weight was measured at day 1 and every two days from day 7 and was taken as a parameter of systemic toxicity. The error bars indicate the SD.

The time course of body weight changes, depicted in **Figure 5**, highlights that treatment with **Pt-3** did not induce ~~any adverse effect, including~~ significant body weight loss, throughout the therapeutic experiment. On the contrary, mice treated with ligand **3** · **HCl** showed a roughly 15% body weight loss and those treated with cisplatin appeared prostrate and showed substantial (about 27%) weight loss.

As shown in **Table 2**, uncoordinated compound **3** · **HCl** ligand tested at 75 mg·kg^{-1} induced a significant tumor growth inhibition that was, however, lower than that promoted by cisplatin. Chemotherapy with **Pt-3** tested at 30 mg·kg^{-1} reduced the tumor mass by roughly 85%, only very slightly lower compared with the reference metallo-drug.

Table 2. *In vivo* antitumor activity toward LLC.

	Daily dose *i.p.* (mg·kg^{-1})	**Average tumor weight (mean ± SD, g)**	**Inhibition of tumor growth (%)**

Control[a]	-	0.582±0.16	-
Pt-3	30	0.086±0.06**	85.2
3 · HCl	75	0.101±0.08**	82.6
Cisplatin	1.5	0.073±0.03**	87.5

[a]vehicle (20% Cremophor EL (v/v), 20% PEG400 (v/v) and 60% saline solution (v/v)); ** p<0.01

Overall, these *in vivo* results confirmed that the coordination of STAT3 inhibitor **3 · HCl** to a platinum moiety, with the aim to develop a dual action agent, led to the obtainment of an effective antitumor metallo-drug. In addition, **Pt-3** and **3 · HCl** appeared to be better tolerated than cisplatin and could be administered at a higher dose.

2.6 Cytotoxic effect of Pt-3 and 3 · HCl on cell lines poorly sensitive to cisplatin.

The cytotoxicity of **Pt-3** was assessed on two additional cancer cell lines less sensitive to cisplatin as compared with HCT-116 cells,[49] namely the breast cancer cell line MCF-7 and the colorectal cancer cell line DLD-1,. As shown in **Figure 6**, **Pt-3** did not affect cell viability of MCF-7 at the concentration range of 1÷25 μM, while a significant inhibition of cell viability was observed for DLD-1 cells at 25 μM concentration. As expected, cisplatin showed a limited cytotoxic efficacy on all three cell lines and with no concentration-dependent action (**Figure 6**). MCF-7 cells resulted particularly resistant to both **Pt-3** and cisplatin.

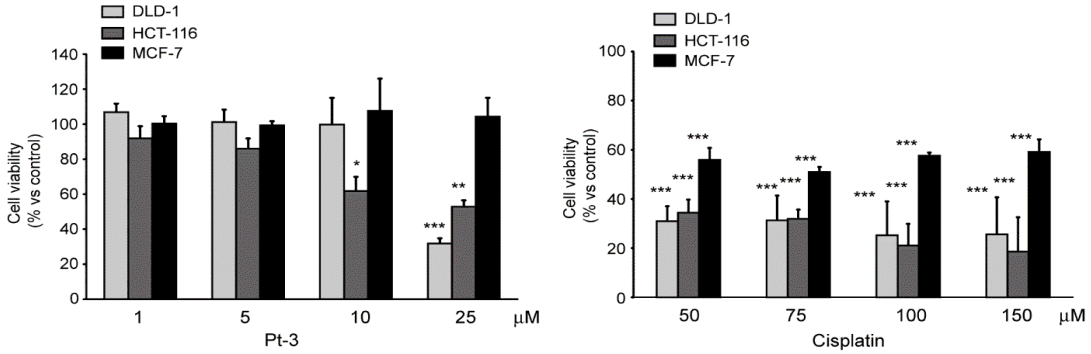

Figure 6. Cytotoxic effects of **Pt-3** complex and cisplatin on DLD-1, HCT-116 and MCF-7 cell lines. Cells were seeded at the density of 40,000/well in a 48 well tray. The day after the medium was replaced with one containing 10% FCS and the reported concentrations of **Pt-3** and cisplatin. After 48 h the cell viability

was estimated by MTT assay. Each bar represents the mean ± SD of three determinations. **Pt-3** and cisplatin *vs* control *P < 0.05;**P < 0.01; ***P < 0.001.

2.7 Intracellular and nuclear accumulation of Pt-3 and induction of p53. To explore the molecular mechanism of action of **Pt-3**, HCT-116 cell line were incubated with the oxadiazole Pt(II) complex (25 and 50 µM) or cisplatin (10 and 25 µM) for 3h and the ^{195}Pt content was determined from both total cell lysates and nuclear DNA preparations. As shown in Figure 7A, a concentration-dependent accumulation of platinum was observed in the DNA extract after incubation with **Pt-3** and cisplatin. However, the efficiency of **Pt-3** to reach the DNA was significantly lower than cisplatin: at 25 µM the amount of Pt measured was 0.48±0.30 ng Pt / µg DNA and 9.0±0.1 ng Pt / µg DNA for **Pt-3** and cisplatin, respectively. By contrast, the ^{195}Pt concentrations were threefold higher in the total cell lysates of HCT-116 incubated with 25 µM of **Pt-3** as compared to 25µM of cisplatin (126.6 ng Pt / µg protein and 42.3 ng Pt / µg protein for **Pt-3** and cisplatin, respectively) (**Figure 7B**).[4] These data suggest that **Pt-3** has a different subcellular distribution than cisplatin, potentially due to an interaction with a cytoplasmic protein.

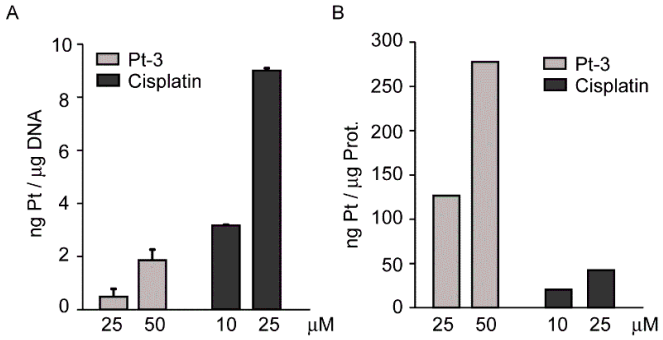

Figure 7. DNA and total intracellular concentrations of ^{195}Pt in HCT-116 cell line incubated with **Pt-3** and cisplatin. Cells were seeded (250,000/35 mm petri dish) and incubated with McCoy's supplemented with 10% FCS; 24 h later the medium was replaced with one containing 10% FCS and indicated concentrations of **Pt-3** or cisplatin. After 3 h, the nuclear DNA and total cell homogenates were prepared and ^{195}Pt concentrations determined by ICPMS and normalized with total DNA (A) and protein contents (B).

Although **Pt-3** interacts less efficiently than cisplatin with nuclear DNA, the incubation of HCT-116 cell line with increasing concentrations of platinum complex for 24 h led to a significant induction of p53, as determined by Western blot analysis (**Figure 8**). These

results suggest that **Pt-3** elicited its cytotoxic effect by interacting with nuclear DNA and thus inducing the expression of p53, similarly to cisplatin.

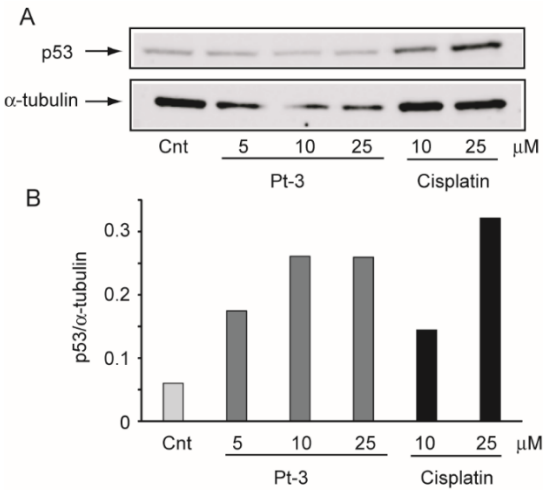

Figure 8. Effect of **Pt-3** on p53 expression in HCT-116 cell line. Cells were seeded (250,000/35 mm petri dish) and incubated with McCoy's supplemented with 10% FCS; 24 h later the medium was replaced with one containing 10% FCS and the reported concentrations of **Pt-3** and cisplatin. The incubation was continued for a further 24 h at 37°C and Western blot analysis was performed from total cell lysates. *α*-tubulin antibody was utilized as loading control.

2.8 DNA binding study. To verify the ability of **Pt-3** to interact with deoxyguanosine rich region of DNA, binding studies were performed with the model nucleobase 9-ethylguanine (9-EtG) by using ^{1}H-NMR.[50, 51] The $N^{7}$of guanine is the putative binding position for the metal centre, thus a downfield chemical shift of the H^{8} next to N^{7} in ^{1}H-NMR should be observed after binding. The experiment was realized using 0.9 % *w/v* NaCl/D_2O solution in DMF-d_7 in order to mimic physiological conditions. In the free 9-EtG, the H^{8} is characterized by a singlet at 7.68 ppm; however, after 12 h it was possible to evidence the presence of a new singlet at 8.32 ppm, thus confirming the binding between **Pt-3** and 9-EtG. (see spectra in SI)

2.9 Glutathione binding study. Glutathione (GSH), a thiol containing tripeptide, is considered to be responsible of the most drug resistance, especially towards platinum drugs.[8, 52, 53] The GSH binding study with **Pt-3** was conducted using 0.9 % *w/v* NaCl/D_2O solution in DMSO-d_6. The ^{1}H-NMR spectrum showed the appearance of two multiplets at 3.04-3.09 and 3.10-3.14 ppm that may be assigned to the methylene protons

next to SH group which are set at 2.60-2.70 and 2.74-2.82 ppm in the unbound form. These signals underlined the interaction between **Pt-3** and GSH thus limiting the bioavailability of the metal compound. (see spectra in SI)

2.10 Effect of Pt-3 on STAT3 expression and phosphorylation. The data obtained with the AlphaScreen-based assay clearly demonstrated the capacity of compounds **3** · **HCl** and **Pt-3** to inhibit the binding between the STAT3-SH2 domain and the phosphotyrosine of the other monomer and, therefore, the STAT3 dimerization. In order to deeply explore the pharmacological activity, we employed a series of experiments aimed at investigating the expression and the phosphorylation state of STAT3. HCT-116 cells were incubated with 25 μM concentration of compounds **3** · **HCl** and **Pt-3** for 24 h and both total protein extracts were prepared. As shown in **Figure 9A**, both compounds did not significantly affect the STAT3 tyrosine phosphorylation state, with a 7.2% and 10.4% inhibition after incubation with **3** · **HCl** and **Pt-3**, respectively.

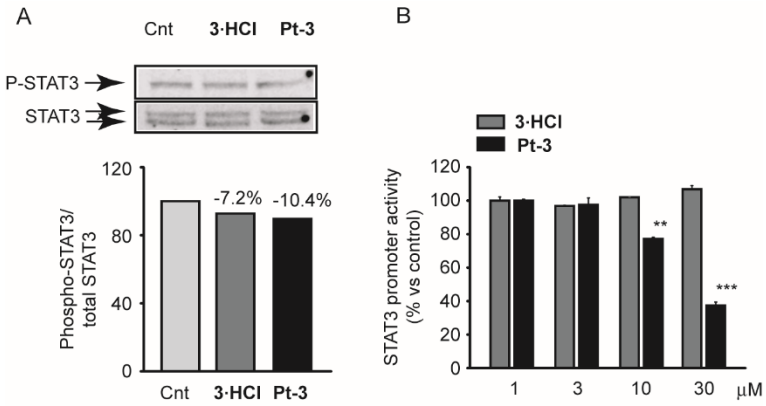

Figure 9. Effect of ligand **3** · **HCl** and **Pt-3** on STAT3 activity in cultured cells. (**A** and **B**) HCT-116 cells were seeded and incubated with McCoy's supplemented with 10% FCS; 24 h later the medium was replaced with one containing 10% FCS and the reported concentrations of **3** · **HCl** and **Pt-3**. The incubation was continued for a further 24 h at 37°C and Western blot analysis (**A**) were performed from total cell lysates. The ratio of phosphoSTAT3/STAT3 signals are shown in the histogram plot. (**B**) Luciferase reporter assay for STAT3 transcriptional activity was performed in HeLa stable cells pre-incubated for 2 h with reported concentrations of **3** · **HCl** and **Pt-3**. The luciferase activity was the stimulated by adding Oncostatin M for 4 h. ** $p < 0.01$; *** $p < 0.001$ *vs* control (Cnt).

The direct measurements of the STAT3 promoter activity by luciferase assay in HeLa cells, showed that **Pt-3** significantly interfered with STAT3 function with an IC_{50} value

equal to 16.7 μM, close to the value observed in the MTT cytotoxicity assay (**Figure 9C** and **Table 1**). On the contrary, compound **3** · **HCl**, did not show any significant activity at the maximal concentration tested (30 μM), confirming its lower cytotoxic effect.

2.11 AlexaFluor488-maleimide labeled STAT3 competition assay. To suggest a possible mechanism by which dimerization disruption occurred in the presence of compound **3** · **HCl** and **Pt-3**, competitive experiments were performed using AlexaFluor488-maleimide labeled STAT3, able to discriminate the interaction site on STAT3 for both the compounds. The results obtained in two different types of experiments are reported in **Figure 10**: a pre-treatment with test compounds assay (**A**) and post-treatment with test compound one (**B**). AlexaFluor488-maleimide reduced **3** · **HCl** and **Pt-3** ability to interact with cysteine residues resulting in lower inhibitory effect. We can speculate that the partial residual activity shown by **Pt-3** might be due to the coordination of platinum metal centre to the thiol groups as expected also in the case of **Pt-1** and **Pt-2**. On the contrary, the lower affinity of compound **3** · **HCl** for cysteines than AlexaFluor488-maleimide led to a total loss of effect. The AlphaScreen-based assay results confirmed **3** · **HCl** and **Pt-3** capability to disrupt STAT3 dimerization without influencing the phosphorylation as reported before by our experimental data (see **Figure 9A**).

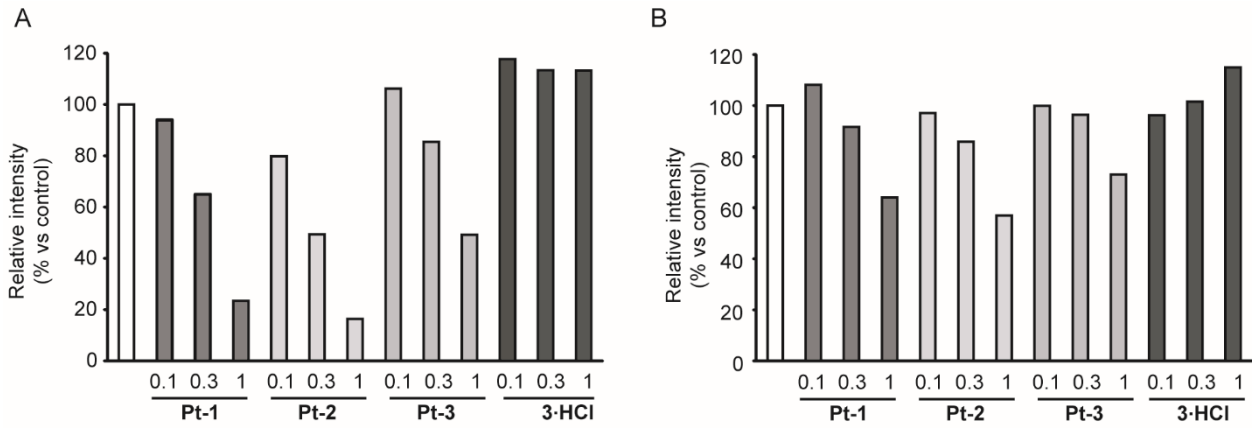

Figure 10. AlexaFluor488-maleimide labeled STAT3 competition assay: a pre-treatment with test compounds assay (**A**) and post-treatment with test compound one (**B**)

3. CONCLUSIONS

Our study aimed to disclose a Pt(II) complex able to interfere with DNA replication and to inhibit STAT3 signaling cascade. In order to achieve this goal, we selected a 3-aminomethyl-1,2,5-oxadiaxole scaffold as ligand for the preparation of Pt(II) complexes. This based-structure was differently substituted to allow the modulation of cytotoxicity and affinity/selectivity for STAT3.

Regarding the *in vitro* experiments, **Pt-1** and **Pt-2** showed a higher inhibitory effect in AlphaScreen-based assay in comparison with **Pt-3** but a negligible cytotoxicity. The 9-EtG results, the induction of p53 determined by Western blot analysis and the presence of ^{195}Pt in DNA extracted from treated HCT-116 cells suggested an interaction with nuclear DNA, although the molecular mechanism of cytotoxicity still needs to be determined. In addition, **Pt-3** did not significantly inhibit the phosphorylation state of STAT3 in HCT-116 cells, but significantly affected the STAT3 promoter activity and thiol modification. All these results supported a possible dual targeting mechanism of **Pt-3**. Digestive LC-MS/MS fragmentation spectroscopy and other biochemical approaches will be employed to fully understand the interaction of **3** · **HCl** and **Pt-3** with specific cysteines of STAT3 domain.

In vivo studies carried out in the highly aggressive Lewis Lung Carcinoma (LLC) model confirmed that the coordination of STAT3 inhibitor **3** · **HCl** to a platinum moiety led to the obtainment of an effective ~~and safe~~ antitumor metallo-drug.

4. EXPERIMENTAL SECTION:

4.1 Materials and Methods. Reagents and solvents were purchased from Sigma-Aldrich and used without further purification. Some reactions involving air-sensitive reagents were performed under nitrogen atmosphere and anhydrous solvents were used when necessary. Reactions were monitored by thin layer chromatography analysis on aluminum-backed Silica Gel 60 plates (70-230 mesh, Merck), using an ultraviolet fluorescent lamp at 254 nm and 365 nm. Visualization was aided by opportune staining reagents. Purification of intermediates and the final compounds was performed by flash chromatography using Geduran® Si 60 (40-63 µm, Merck). HCT-116 cell line (colorectal cancer) were cultured in McCoy's media, the DLD-1 (colorectal cancer) and MCF-7 were cultured in Dulbecco's modified eagle's medium (DMEM) with glutamine. All the media

were supplemented with penicillin (10,000 U/mL), streptomycin (10 mg/mL), nonessential amino acid and 10% Fetal Calf Serum (FCS). The same media was utilized for the experiments where cells were incubated with newly synthesized compounds dissolved in DMSO. The same volume of solvent was added to control conditions and did not exceed 0.5% v/v.: HCT 116 ATCC® number CCL 247™; MCF7: ATCC® number HTB-22™, DLD1: ATCC® number CCL-221™, HELA: ATCC® number CCL-2™ and STAT3-HeLa SL-0003 (from Signosis).

4.2 Physical Measurements. ^{1}H and ^{13}C NMR spectra were recorded in $CDCl_3$, CD_3OD, DMSO-d_6 or DMF-d_7 on Bruker DRX Avance 300 MHz or on a Variant 300 MHz Oxford equipped with a non-reverse probe at 25° C. Chemical shifts (in ppm) were referenced to residual solvent proton/carbon peak. Chemical shifts are expressed as δ (ppm). Multiplicity is reported as *s* (singlet), *br s* (broad singlet), *d* (double), *t* (triplet), *q* (quartet), *m* (multiplet), *dd* (double of doublets), *dt* (doublet of triplets). The coupling constants (J-values) are given in Hertz (Hz). All spectroscopic data match the assigned structures. FTIR spectra were collected by using a Perkin Elmer (MA, USA) FTIR Spectrometer “Spectrum One” in a spectral region between 4000 and 450 cm^{-1} and analysed by transmittance technique with 32 scansions and 4 cm^{-1} resolution. ESI-MS analyses were performed by using a Thermo Finnigan (MA, USA) LCQ Advantage system MS spectrometer with an electronspray ionisation source and an ‘Ion Trap’ mass analyser. The MS spectra were obtained by direct infusion of a sample solution in MeOH under ionisation, ESI positive. Log P_{ow}’s values and purity were evaluated with Partisil C18-ODS reversed-phase HPLC column with Merck-Hitachi L-7100 equipped with Detector UV6000LP. Elemental analyses were performed using a Perkin Elmer SeriesII/CHNS/O 2400 Analyzer. ICP-MS data were recorded with BRUKER aurora M90 ICP-MS (MA, USA).

4.3 CHEMISTRY

4.3.1 General procedure for the synthesis of platinum complexes Pt-1, Pt-2 and Pt-3

An amount of K_2PtCl_4 (1 mmol) was dissolved in 10 mL of distilled water. Ligand (1.1 mmol) when available in dihydrochloride form was preventively neutralized with $NaHCO_3$ aqueous solution and was dropped into palatinate solution. 4 M HCl (10 equivalents) was added and the mixture was refluxed under nitrogen atmosphere for 12 h. After cooling to room temperature, the product was filtered as a solid and washed extensively with water. The precipitate was then dissolved in diethyl ether and crystallized for slow diffusion of hexane.

Pt-1*:* pale-yellow solid, 62% yield. Chemical Formula: $C_4H_7Cl_2N_3OPt$. Molecular Weight: 377.96 g/mol. ^{1}H NMR (300 MHz, DMF-d_7) δ 6.72 (br, 2H), 4.34 (t, J = 6.3 Hz, 2H), 2.61 (s, 3H) ppm. ^{13}C NMR (75 MHz, DMF-d_7) 163.18, 153.94, 42.79, 8.64 ppm. ^{195}Pt NMR (300 MHz, DMF-d_7) δ -2065 ppm. Elemental analysis for $C_4H_7Cl_2N_3OPt$: calculated C, 12.67; H, 1.81; N, 11.09; found C, 12.72; H, 1.78; N, 10.98, IR v = 3217, 3188, 3103, 1586, 1567, 1426, 1376, 1201, 1050, 970 cm^{-1}, MS (ESI) *m/z* 365.9 $[M\text{-}Cl+Na]^+$.

Pt-2: brown solid, 45% yield. Chemical Formula: $C_9H_8Cl_3N_3OPt$. Molecular Weight: 473.94 g/mol. ^{1}H NMR (300 MHz, DMF-d_7) δ 7.98 (d, J = 8.8 Hz, 2H), 7.76 (d, J = 8.8 Hz, 2H), 6.94 (br, 2H), 4.61 (t, J = 6.0 Hz, 2H) ppm. ^{13}C NMR (75 MHz, DMF-d_7) 137.78, 130.49, 130.19, 125.25, 123.31, 116.47, 44.35 ppm. ^{195}Pt NMR (300 MHz, DMF-d_7) δ -2075 ppm. Elemental analysis for $C_9H_8Cl_3N_3OPt$: calculated C, 22.93; H, 1.70; N, 8.84; found C, 23.01; H, 1.75; N, 8.89, IR v = 3243, 3204, 2962, 2919, 1602, 1567, 1464, 1261, 1096, 1016, 802 cm^{-1}, MS (ESI) *m/z* 461.9 $[M\text{-}Cl+Na]^+$.

Pt-3*:* olive-green solid, 61% yield. Chemical Formula: $C_{16}H_{12}Cl_3N_3O_2Pt$. Molecular Weight: 577.96 g/mol. ^{1}H NMR (300 MHz, $CDCl_3$) δ 7.77 (d, J = 8.5 Hz, 2H), 7.50-7.44 (m, 5H), 7.25-7.21 (m, 2H), 6.20 (t, J = 5.8Hz, 1H), 5.46-5.41 (m, 1H), 4.88-4.85 (m, 1H) ppm. ^{13}C NMR (75 MHz, $CDCl_3$) 191.27, 152.84, 149.45, 138.06, 135.09, 132.73, 130.44, 130.35, 130.23, 130.19, 129.60, 129.51, 129.47, 129.32, 129.23, 128.93, 55.15 ppm. ^{195}Pt NMR (300 MHz, $CDCl_3$) δ -2068 ppm. Elemental analysis for $C_{16}H_{12}Cl_3N_3O_2Pt$: calculated C, 33.35; H, 2.13; N, 7.45; found C, 33.58; H, 2.18; N, 7.54, IR v = 3145, 3078, 2931, 1697, 1597, 1448, 1261, 1216, 1094, 995, 960, 834, 688 cm^{-1},MS (ESI) *m/z* 578.5 $[M+H]^+$.

4.3.2 Crystallization, data collection and structural determination.

Single crystals of **Pt-1** suitable for X-ray structure analysis were obtained by slow evaporation of a solution ~~solution~~ 33% MeOH:water at room temperature. The crystals were small yellow needles. Intensity data were collected at room temperature on a Bruker Axs CCD-based three cycle diffractometer**,** using graphite-monochromatized Mo-K radiation (λ= 0.71073 Å).

X-ray diffraction data in the θ range 2-25° were collected acquiring 4 sets of 600 bidimensional CCD frames with the following operative conditions: omega rotation axis, scan width 0.3°, acquisition time 40 s, sample-to-detector distance 50 mm, phi angle fixed at four different values (0°, 90°, 180°, 270°) for the four different sets.

Omega-rotation frames were processed with the SAINT software[54] for data reduction (including intensity integration, background, Lorentz and polarization corrections) and for determination of accurate unit-cell dimensions, obtained by least-squares refinement of the positions of 8049 independent reflections with I > 10σ(I) in the θ range 2-24°. Absorption effects were empirically evaluated by the SADABS software[55] and absorption correction was applied to the data (0.367 and 0.602 min and max transmission factor).

The structure was solved by direct methods (*SIR-97*[56]) and completed by iterative cycles of full-matrix least squares refinement on F_o^2 and ΔF synthesis using the *SHELXL-97*[57] program (*WinGX* suite).[37] All non-H-atoms were refined anisotropically. The H-atoms positions were introduced in calculated positions in their described geometries and allowed to ride on the attached carbon atom with fixed isotropic thermal parameters. Geometrical calculations were carried out with the program PARST.[58] The crystal data are given below. CCDC-1478539 contains the supplementary crystallographic data for this paper. These data can be obtained free of charge *via* www.ccdc.cam.ac.uk/conts/retrieving.html (or from the Cambridge Crystallographic Data Centre, 12, Union Road, Cambridge CB21EZ, UK; fax: ++44 1223 336 033; or deposit@ccdc.cam.ac.uk).

Crystal data: $C_4\ H_7\ O_1\ Pt_1\ Cl_2\ N_3$, M_r = 379.01 g/mol, Trigonal, Space group *R-3* a= 39.836(2) Å, *c* = 6.724(3) Å, *V* = 9240.8(5) Å^3, *Z* = 12, D_{calc} = 2.439 Mg/m^3, F(000) = 6120, *R* = 0.026 (reflections collected/unique = 3614/3228), *wR2* = 0.031, *T* = 293(2)K, *GOF* = 1.057. The reflections were collected in the range 1.02° ≤ θ ≤ 25.03° (limiting indices = -

47≤h≤47, -47≤k≤47, -8≤l≤7) employing a 0.01 x 0.02 x 0.01 mm^3 crystal. The residual positive and negative electron densities in the final map were 0.950 and –0.540 $eÅ^{-3}$.

4.3.3 Stability test. The stability study of complexes (**Pt-1**, **Pt-2** and **Pt-3**) was performed under physiological conditions through UV-vis spectroscopy at their respective λ_{max}. Stock solutions were diluted to a final concentration of 100 µM with 1 % DMF. The UV-vis peak profile of the sample was monitored for 48 h at 4 h intervals.

4.3.4 Log P_{ow} determination. RP-HPLC analysis were performed to correlate the hydrophobicity of the compounds and the Pt(II) complexes with their retention time. The chromatograms were registered using Partisil C18-ODS reversed-phase HPLC column at 25 °C and water/acetonitrile (60:40) as mobile phase with KI as internal standard (flow rate: 1 mL/min; λ= 230 nm). For platinum complexes the same column was used and water (15 mM HCOOH)/MeOH (70:30) mobile phase with KI as internal standard (flow rate of 1 mL/min, λ= 210 nm).[41-43, 59] The calibration curve was realized in comparison with reference compounds chosen in OECD guideline.[54]

4.4 BIOLOGY

4.4.1 Cell culture. The following human cancer cell lines have been utilized in the study: HCT-116 (colorectal cancer), DLD1 (colorectal cancer), and MCF-7 (breast cancer). All cultured media were supplemented with penicillin (10,000 U/mL), streptomycin (10 mg/mL), non-essential amino acid and 10% Fetal Calf Serum (FCS). Dulbecco's modified eagle's medium (DMEM) with glutamine was utilized for MCF-7, and DLD-1 cell lines and McCoy's for HCT-116. Cells were incubated with newly synthesized compounds dissolved in DMSO. The same volume of solvent were added to control conditions and did not exceed 0.5% v/v.

4.4.2 MTT-assay. The MTT assay was performed according to literature data.[29, 49]

4.4.3 AlphaScreen-based assay. It is a bead-based nonradioactive assay system for detecting biomolecular interactions in a microtiter plate format. Binding of biological

partners brings donor and acceptor beads into close proximity and as a result, a fluorescent signal between 520 and 620 nm is produced. The AlphaScreen-based assays[23, 60] were performed in a final reaction volume of 25 µL of the assay buffer containing 10 mM HEPES–NaOH (pH 7.4), 50 mM NaCl, 1 mM EDTA (pH 8.0), 0.1% NP-40, and 10 ng/µL BSA in a 96-well microtiter plate at 25 °C. Phospho-Tyr (pTyr) peptide probes used in this study were 5-carboxyfluorescein (FITC)-GpYLPQTV for STAT3 and (FITC)-GpYDKPHVL for STAT1. Firstly, 75 nM of each SH2-containing protein was incubated with the test compound for 15 min. Each protein sample was then incubated for 90 min with 50 nM of its corresponding FITC-pTyr peptide, and mixed with streptavidin coated donor beads and anti-FITC acceptor beads simultaneously before detection at 570 nm using EnVison Xcite (PerkinElmer).

4.4.4 ***In vivo*** **antitumor activity in Lewis Lung Carcinoma.** All experiments were performed according to D.L.G.S. 26/2014 which warrants care of experimental animals in Italy. The research project was approved by the Italian Health Department according to the art. 7 of above mentioned D.L. The LLC cell line was purchased from ECACC, United Kingdom. The LLC cell line was maintained in DMEM (Euroclone) supplemented with 10% heat-inactivated fetal bovine serum (FBS; Euroclone), 10 mM L-glutamine, 100 U mL^{-1} penicillin, and 100 µg mL^{-1} streptomycin in a 5% CO_2 air incubator at 37 °C. The LLC was implanted intramuscularly (im) as a 2×10^6 cell inoculum into the right hind leg of 8 week old male and female C57BL mice (24 ± 3 g body weight). After 24 h from tumor implantation, mice were randomly divided into five groups (8 animals per group, 10 controls). From day 7 after tumor inoculation (visible tumor) animals were treated daily with a single dose of compound **3** · **HCl** and of **Pt-3** complex (75 mg kg^{-1} and 30 mg kg^{-1}, respectively, dissolved in a vehicle solution composed of 20% Cremophor EL (v/v), 20% PEG400 (v/v) and 60% saline solution (v/v)) or with a daily ip dose of cisplatin (1.5 mg kg^{-1} in 0.9% NaCl solution). At day 15, animals were sacrificed, the legs were amputated at the proximal end of the femur, and the inhibition of tumor growth was determined according to the difference in weight of the tumor-bearing leg and the healthy leg of the animals expressed as a percentage referred to the control animals. Body weight was

measured at day 1 and every two days from day 7, and was taken as a parameter for systemic toxicity. All the values are the means ± SD of not less than three measurements.

4.4.5 Determination of intracellular and DNA-bound Pt concentrations. For the determination of total intracellular ^{195}Pt concentrations, cells were homogenates with lysis buffer containing 0.5% NP-40, 150 mM NaCl and 50 mM Tris-HCl at pH 7.5. The cell monolayer was three times with PBS before the incubation with the lysis buffer for 30 min at 4°C. Cell lysates were treated then cleared by centrifugation at 14,000g for 10 min, and the ^{195}Pt concentrations determined by ICP-MS. The data were normalized with the protein concentrations were determined using the BCA protein assay (Thermo scientific, Rockford, IL USA). The ^{195}Pt concentration bound to DNA was estimated from nuclear DNA extracted as previously described.[29] The data were normalized with DNA concentrations determined by spectrophotometer determination with NanoDrop system.

4.4.6 Binding study with 9-ethylguanine and GSH. The binding studies were directly conducted in NMR tube preparing 1 eq. of **Pt-3** in 20 % of 0.9 % *w/v* NaCl-D_2O solution in DMSO-d_6. 1eq. of 9-ethylguanine or GSH was added to a solution. The samples were evaluated at different times by ^{1}H-NMR analysis.

4.4.7 Western blot analysis. Cells were washed twice with PBS and lysed by incubation with a solution of 50 mM Tris pH 7.5, 150 mM NaCl, 0.5% Nonidet-P40, containing a protease inhibitor cocktails (Sigma Aldrich, Milan, Italy) for 30 min on ice. Cell lysates were then cleared by centrifugation at 14,000g for 10 min.[61] Protein samples were separated by SDS-PAGE under reducing conditions, transferred to nitrocellulose membrane (GE Healthcare Little Chalfont, Buckinghamshire, UK) and subsequently immunoblotted with primary antibody following appropriate secondary fluorescently labeled antibody and acquired with the Odissey FC system (LI-COR). Quantitative densitometric analyses were performed with Image Studio software (LI-COR). The following antibodies were utilized: monoclonal antibody anti p53 and β-tubulin (SIGMA), anti-pSTAT3 (Abcam) and anti-STAT3 (Santa-Cruz Biotechnology).

4.4.8 Luciferase reporter gene assay. STAT3 reporter HeLa stable cells (Signosis Inc) were incubated in a 96-well microplate for 24 h. Cells were pretreated with test compounds for 2 h, and 10 ng/ml (w/v) of Oncostatin M were applied and incubated for 4 h. Cells were washed with medium not supplemented with phenol red, and Steady-Glo® reagent (Promega) was applied. After 15 min incubation, the signals were detected by ARVO Light 1420 (PerkinElmer Life Sciences). The relative signal intensity was calculated in each well as the ratio for the mean signal of vehicle. In parallel with the procedure, CellTiter-Glo (CTG) Luminescent Cell Viability Assay (Promega) was performed for checking the viability of the cells.

4.4.9 AlexaFluor488-maleimide labeled STAT3 competition assay.

Pre-treatment: The recombinant human STAT3 protein (0.3 μM) was incubated with the test compound in 100 mM HEPES for 2 h at 25℃. Alexa Fluor 488 C5 maleimide (50 μM) was added to the mixture and incubated for further 2h at 25℃. Samples were diluted in SDS-PAGE sample buffer without 2-mercaptoethanol and run on an SDS-PAGE gel. Fluorescence of Alexa-labeled STAT3 was analyzed with FUJIFILM LAS-3000 image analyzer (excitation/emission: 493/516 nm)

Post-treatment: The recombinant human STAT3 protein (0.3 μM) was incubated with Alexa Fluor 488 C5 maleimide (50 μM) in 100 mM HEPES for 2 h at 25℃. The test compound was added to the mixture and incubated for further 2h at 25℃. Samples were diluted in SDS-PAGE sample buffer without 2-mercaptoethanol and run on an SDS-PAGE gel. Fluorescence of Alexa-labeled STAT3 was analyzed with FUJIFILM LAS-3000 image analyzer (excitation/emission: 493/516 nm).

4.4.10 Statistical analysis

All data shown are representative of at least three replicate experiments. Data are expressed as mean ± SD. Statistical analyses were performed using the unpaired Student's t test. P values <0.05 were considered significant. The concentration of compounds required to reduce by 50% the cell viability (EC_{50}) was calculated by nonlinear regression curve (SigmaPlot software; Systat Software, Inc., Point Richmond, CA).

AUTHOR INFORMATION

Corresponding Author

*isabella.rimoldi@unim.it, +39 0250314609; nicola.ferri@unipd.it, +39 0498275080; arianna.gelain@unimi.it, +39 0250319369.

Author Contributions

±These authors contributed equally.

Acknowledgments

This study was supported by funds from PRIN 2010-2011. Authors also thank Fondazione Confalonieri (Fellowship 2015) for the financial support. BM Kwon was supported by the Bio-Synergy Research Project (2012M3A9C4048777).

REFERENCES

[1] R.A. Alderden, M.D. Hall, T.W. Hambley, The Discovery and Development of Cisplatin, J. Chem. Educ., 83 (2006) 728.
[2] B. Rosenberg, L. Vancamp, J.E. Trosko, V.H. Mansour, Platinum Compounds: a New Class of Potent Antitumour Agents, Nature, 222 (1969) 385-386.
[3] F. Arnesano, G. Natile, Mechanistic insight into the cellular uptake and processing of cisplatin 30 years after its approval by FDA, Coord. Chem. Rev., 253 (2009) 2070-2081.
[4] E. Raymond, S. Faivre, S. Chaney, J. Woynarowski, E. Cvitkovic, Cellular and Molecular Pharmacology of Oxaliplatin1, Mol Cancer Ther, 1 (2002) 227-235.
[5] L. Kelland, The resurgence of platinum-based cancer chemotherapy, Nat Rev Cancer, 7 (2007) 573-584.
[6] A.J. Di Pasqua, J. Goodisman, J.C. Dabrowiak, Understanding how the platinum anticancer drug carboplatin works: From the bottle to the cell, Inorg. Chim. Acta, 389 (2012) 29-35.
[7] C.A. Rabik, M.E. Dolan, Molecular mechanisms of resistance and toxicity associated with platinating agents, Cancer Treatment Reviews, 33 (2007) 9-23.
[8] M.A. Fuertes, C. Alonso, J.M. Pérez, Biochemical Modulation of Cisplatin Mechanisms of Action: Enhancement of Antitumor Activity and Circumvention of Drug Resistance, Chem. Rev., 103 (2003) 645-662.
[9] Y. Jung, S.J. Lippard, Direct Cellular Responses to Platinum-Induced DNA Damage, Chem. Rev., 107 (2007) 1387-1407.
[10] V.M. Gonzalez, M.A. Fuertes, C. Alonso, J.M. Perez, Is Cisplatin-Induced Cell Death Always Produced by Apoptosis?, Mol Pharmacol, 59 (2001) 657-663.
[11] M. Fraser, B.M. Leung, X. Yan, H.C. Dan, J.Q. Cheng, B.K. Tsang, p53 Is a Determinant of X-Linked Inhibitor of Apoptosis Protein/Akt-Mediated Chemoresistance in Human Ovarian Cancer Cells, Cancer Res, 63 (2003) 7081-7088.
[12] J.E. Darnell, Transcription factors as targets for cancer therapy, Nat Rev Cancer, 2 (2002) 740-749.

[13] S. Fletcher, J. Turkson, P.T. Gunning, Molecular Approaches towards the Inhibition of the Signal Transducer and Activator of Transcription 3 (Stat3) Protein, ChemMedChem, 3 (2008) 1159-1168.
[14] C.-M. Che, F.-M. Siu, Metal complexes in medicine with a focus on enzyme inhibition, Curr. Opin. Chem. Biol., 14 (2010) 255-261.
[15] J. Bromberg, Stat proteins and oncogenesis, The Journal of Clinical Investigation, 109 (2002) 1139-1142.
[16] J. Schust, B. Sperl, A. Hollis, T.U. Mayer, T. Berg, Stattic: A Small-Molecule Inhibitor of STAT3 Activation and Dimerization, Chemistry & Biology, 13 (2006) 1235-1242.
[17] Y. Pan, F. Zhou, R. Zhang, F.X. Claret, Stat3 Inhibitor Stattic Exhibits Potent Antitumor Activity and Induces Chemo- and Radio-Sensitivity in Nasopharyngeal Carcinoma, PLoS ONE, 8 (2013) e54565.
[18] C.L. Yu, D.J. Meyer, G.S. Campbell, A.C. Larner, C. Carter-Su, J. Schwartz, R. Jove, Enhanced DNA-binding activity of a Stat3-related protein in cells transformed by the Src oncoprotein, Science (New York, N.Y.), 269 (1995) 81-83.
[19] D.P. Ball, A.M. Lewis, D. Williams, D. Resetca, D.J. Wilson, P.T. Gunning, Signal transducer and activator of transcription 3 (STAT3) inhibitor, S3I-201, acts as a potent and non-selective alkylating agent, Oncotarget, 7 (2016) 20669-20679.
[20] L. Li, P.E. Shaw, A STAT3 dimer formed by inter-chain disulphide bridging during oxidative stress, Biochemical and Biophysical Research Communications, 322 (2004) 1005-1011.
[21] J. Boström, A. Hogner, A. Llinàs, E. Wellner, A.T. Plowright, Oxadiazoles in Medicinal Chemistry, J. Med. Chem., 55 (2012) 1817-1830.
[22] D. Masciocchi, A. Gelain, S. Villa, F. Meneghetti, D. Barlocco, Signal transducer and activator of transcription 3 (STAT3): a promising target for anticancer therapy, Future Medicinal Chemistry, 3 (2011) 567-597.
[23] K. Matsuno, Y. Masuda, Y. Uehara, H. Sato, A. Muroya, O. Takahashi, T. Yokotagawa, T. Furuya, T. Okawara, M. Otsuka, N. Ogo, T. Ashizawa, C. Oshita, S. Tai, H. Ishii, Y. Akiyama, A. Asai, Identification of a New Series of STAT3 Inhibitors by Virtual Screening, ACS Med. Chem. Lett., 1 (2010) 371-375.
[24] T. Ashizawa, Akiyama, Y., Miyata, H., Iizuka, A., Komiyama, M., Kume, A., Omiya, M., Sugino, T., Asai, A., Hayashi, N., Mitsuya, K., Nakasu, Y., Yamaguchi, K., Effect of the STAT3 inhibitor STX-0119 on the proliferation of a temozolomide-resistant glioblastoma cell line, International Journal of Oncology, 1 (2014) 411-418.
[25] D.C. Han, M.-Y. Lee, K.D. Shin, S.B. Jeon, J.M. Kim, K.-H. Son, H.-C. Kim, H.-M. Kim, B.-M. Kwon, 2′-Benzoyloxycinnamaldehyde Induces Apoptosis in Human Carcinoma via Reactive Oxygen Species, Journal of Biological Chemistry, 279 (2004) 6911-6920.
[26] D.-S. Shin, D. Masciocchi, A. Gelain, S. Villa, D. Barlocco, F. Meneghetti, A. Pedretti, Y.-M. Han, D.C. Han, B.-M. Kwon, L. Legnani, L. Toma, Synthesis, modeling, and crystallographic study of 3,4-disubstituted-1,2,5-oxadiazoles and evaluation of their ability to decrease STAT3 activity, MedChemComm, 1 (2010) 156-164.
[27] F. Meneghetti, S. Villa, D. Masciocchi, D. Barlocco, L. Toma, D.-C. Han, B.-M. Kwon, N. Ogo, A. Asai, L. Legnani, A. Gelain, Ureido-Pyridazinone Derivatives: Insights into the Structural and Conformational Properties for STAT3 Inhibition, Eur. J. Org. Chem., (2015) 4907-4912.
[28] D. Masciocchi, S. Villa, F. Meneghetti, A. Pedretti, D. Barlocco, L. Legnani, L. Toma, B.-M. Kwon, S. Nakano, A. Asai, A. Gelain, Biological and computational evaluation of an oxadiazole

derivative (MD77) as a new lead for direct STAT3 inhibitors, MedChemComm, 3 (2012) 592-599.
[29] N. Ferri, G. Facchetti, S. Pellegrino, E. Pini, C. Ricci, G. Curigliano, I. Rimoldi, Promising antiproliferative platinum(II) complexes based on imidazole moiety: synthesis, evaluation in HCT-116 cancer cell line and interaction with Ctr-1 Met-rich domain, Bioorg Med Chem, 23 (2015) 2538-2547.
[30] I. Rimoldi, G. Facchetti, G. Lucchini, E. Castiglioni, S. Marchianò, N. Ferri, In vitro anticancer activity evaluation of new cationic platinum(II) complexes based on imidazole moiety, Bioorg. Med. Chem., 25 (2017) 1907-1913.
[31] D.M. Fisher, R.R. Fenton, J.R. Aldrich-Wright, In vivo studies of a platinum(ii) metallointercalator, Chem. Commun., (2008) 5613-5615.
[32] E. Gabriele, F. Porta, G. Facchetti, C. Galli, A. Gelain, F. Meneghetti, I. Rimoldi, S. Romeo, S. Villa, C. Ricci, N. Ferri, A. Asai, D. Barlocco, A. Sparatore, Synthesis of new dithiolethione and methanethiosulfonate systems endowed with pharmaceutical interest, Arkivoc, part ii (2017) 235-250.
[33] G.V. Sagar Reddy, G.V. Rao, R.V.K. Subramanyam, D.S. Iyengar, A New Novel and Practical One Pot Methodology for Conversion of Alcohols to Amines, Synth. Commun., 30 (2000) 2233-2237.
[34] R. Dreos, P. Siega, S. Scagliola, L. Randaccio, G. Nardin, C. Tavagnacco, M. Bevilacqua, Synthesis, Characterization, and Electrochemical Properties of Dinuclear Complexes Assembled from Asymmetric CoIII Bis(dioximates) and Boronic Acids, Eur. J. Inorg. Chem., 2005 (2005) 3936-3944.
[35] T.J. Egan, K.R. Koch, P.L. Swan, C. Clarkson, D.A. Van Schalkwyk, P.J. Smith, In Vitro Antimalarial Activity of a Series of Cationic 2,2â€˜-Bipyridyl- and 1,10-Phenanthrolineplatinum(II) Benzoylthiourea Complexes, J. Med. Chem., 47 (2004) 2926-2934.
[36] S.J. Berners-Price, L. Ronconi, P.J. Sadler, Insights into the mechanism of action of platinum anticancer drugs from multinuclear NMR spectroscopy, Prog. Nucl. Magn. Reson. Spectrosc., 49 (2006) 65-98.
[37] L.J. Farrugia, WinGX suite for small-molecule single-crystal crystallography, J. Appl. Crystallogr., 32 (1999) 837-838.
[38] J. Llorca, E. Molins, E. Espinosa, I. Mata, C. Miravitlles, G. Cervantes, A. Caubet, V. Moreno, Dichloro(d-methionine-N,S)platinum(II) at 130 K, Acta Crystallographica Section C, 57 (2001) 804-806.
[39] A. Bondi, van der Waals Volumes and Radii, The Journal of Physical Chemistry, 68 (1964) 441-451.
[40] W. Lu, M.C.W. Chan, N. Zhu, C.-M. Che, C. Li, Z. Hui, Structural and Spectroscopic Studies on Pt···Pt and π–π Interactions in Luminescent Multinuclear Cyclometalated Platinum(II) Homologues Tethered by Oligophosphine Auxiliaries, J. Am. Chem. Soc., 126 (2004) 7639-7651.
[41] J.A. Platts, D.E. Hibbs, T.W. Hambley, M.D. Hall, Calculation of the Hydrophobicity of Platinum Drugs, J. Med. Chem., 44 (2000) 472-474.
[42] S.P. Oldfield, M.D. Hall, J.A. Platts, Calculation of Lipophilicity of a Large, Diverse Dataset of Anticancer Platinum Complexes and the Relation to Cellular Uptake, J. Med. Chem., 50 (2007) 5227-5237.
[43] I.V. Tetko, I. Jaroszewicz, J.A. Platts, J. Kuduk-Jaworska, Calculation of lipophilicity for Pt(II) complexes: Experimental comparison of several methods, J. Inorg. Biochem., 102 (2008) 1424-1437.

[44] M. Reist, L.H. Christiansen, P. Christoffersen, P.-A. Carrupt, B. Testa, Low configurational stability of amfepramone and cathinone: Mechanism and kinetics of chiral inversion, Chirality, 7 (1995) 469-473.
[45] S. Mohr, J.A. Weiß, J. Spreitz, M.G. Schmid, Chiral separation of new cathinone- and amphetamine-related designer drugs by gas chromatography–mass spectrometry using trifluoroacetyl-l-prolyl chloride as chiral derivatization reagent, Journal of Chromatography A, 1269 (2012) 352-359.
[46] M. Kortylewski, R. Jove, H. Yu, Targeting STAT3 affects melanoma on multiple fronts, Cancer and Metastasis Reviews, 24 (2005) 315-327.
[47] J.S. McMurray, J. Klostergaard, Chapter 7 - STAT3 Signaling in Cancer: Small Molecule Intervention as Therapy?, in: Anti-Angiogenesis Drug Discovery and Development, Elsevier, 2014, pp. 216-267.
[48] V. Gandin, A. Trenti, M. Porchia, F. Tisato, M. Giorgetti, I. Zanusso, L. Trevisi, C. Marzano, Homoleptic phosphino copper(i) complexes with in vitro and in vivo dual cytotoxic and anti-angiogenic activity, Metallomics, 7 (2015) 1497-1507.
[49] N. Ferri, S. Cazzaniga, L. Mazzarella, G. Curigliano, G. Lucchini, D. Zerla, R. Gandolfi, G. Facchetti, M. Pellizzoni, I. Rimoldi, Cytotoxic effect of (1-methyl-1H-imidazol-2-yl)-methanamine and its derivatives in PtII complexes on human carcinoma cell lines: A comparative study with cisplatin, Bioorg. Med. Chem., 21 (2013) 2379-2386.
[50] T.C. Johnstone, S.J. Lippard, The Chiral Potential of Phenanthriplatin and Its Influence on Guanine Binding, J. Am. Chem. Soc., 136 (2014) 2126-2134.
[51] D. Lemaire, M.-H. Fouchet, J. Kozelka, Effect of platinum N7-binding to deoxyguanosine and deoxyadenosine on the H8 and H2 chemical shifts. A quantitative analysis, J. Inorg. Biochem., 53 (1994) 261-271.
[52] Y. Min, C.-Q. Mao, S. Chen, G. Ma, J. Wang, Y. Liu, Combating the Drug Resistance of Cisplatin Using a Platinum Prodrug Based Delivery System, Angew. Chem. Int. Ed., 51 (2012) 6742-6747.
[53] B.A.J. Jansen, J. Brouwer, J. Reedijk, Glutathione induces cellular resistance against cationic dinuclear platinum anticancer drugs, J. Inorg. Biochem., 89 (2002) 197-202.
[54] OECD Guideline for Testing of Chemicals-Partition Coefficient (n-octanol/water), High Performance Liquid Chromatography (HPLC) Method, in.
[55] L. Krause, R. Herbst-Irmer, G.M. Sheldrick, D. Stalke, Comparison of silver and molybdenum microfocus X-ray sources for single-crystal structure determination, J. Appl. Crystallogr., 48 (2015) 3-10.
[56] A. Altomare, M.C. Burla, M. Camalli, G.L. Cascarano, C. Giacovazzo, A. Guagliardi, A.G.G. Moliterni, G. Polidori, R. Spagna, SIR97: a new tool for crystal structure determination and refinement, J. Appl. Crystallogr., 32 (1999) 115-119.
[57] G.M. Sheldrick, in, SHELX97, Programs for Crystal Structure Analysis (Release 97-2); University of Göttingen, Germany, 1998.
[58] M. Nardelli, PARST95 - an update to PARST: a system of Fortran routines for calculating molecular structure parameters from the results of crystal structure analyses, J. Appl. Crystallogr., 28 (1995) 659.
[59] J.A. Platts, S.P. Oldfield, M.M. Reif, A. Palmucci, E. Gabano, D. Osella, The RP-HPLC measurement and QSPR analysis of log Po/w values of several Pt(II) complexes, J. Inorg. Biochem., 100 (2006) 1199-1207.

[60] Y. Uehara, M. Mochizuki, K. Matsuno, T. Haino, A. Asai, Novel high-throughput screening system for identifying STAT3–SH2 antagonists, Biochemical and Biophysical Research Communications, 380 (2009) 627-631.
[61] C.M. Greco, M. Camera, L. Facchinetti, M. Brambilla, S. Pellegrino, M.L. Gelmi, E. Tremoli, A. Corsini, N. Ferri, Chemotactic effect of prorenin on human aortic smooth muscle cells: a novel function of the (pro)renin receptor, Cardiovascular Research, 95 (2012) 366-374.

LISTS OF CAPTIONS

Figure 1. New Pt(II) complexes.

Figure 2. Ligands and their corresponding Pt(II) complexes.

Scheme 1. Reagents and conditions: *i)* NaN_3, Ph_3P, CCl_4/DMF (1:4), 90°C, 5 h; *ii)* Pd/C, H_2, MeOH, 20 atm, 4 h; *iii)* 2 M HCl in Et_2O.

Scheme 2. Reagents and conditions *i) t*-BuONO, TMSCl, dry THF/DCM, -20°C to rt, 12 h; *ii)* $NH_2OH{\cdot}HCl$, NaOH, H_2O, reflux, 3 h; *iii)* KOH, Cs_2CO_3, ethylen glycol, 160°C, 1.5 h; *iv)* 2.5 M *n*-BuLi in hexane, methyl benzoate, dry THF, -55°C for 1 h, then rt for 12 h; *v) t*-BuONO, TMSCl, dry THF, -20°C to rt, 12 h; *vi)* Zn, TFA, rt, 40 min; *vi)* 2 M HCl in Et_2O.

Scheme 3. Reagents and conditions: *i)* K_2PtCl_4, 4 M HCl, H_2O, reflux, 2 h.

Figure 3: ORTEP[37] view of one of the two molecules present in the asymmetric unit of **Pt-1**, showing the arbitrary atom labeling scheme. Ellipsoids are drawn at 40% probability level and H atoms are shown as spheres of arbitrary radius. Selected averaged bond distances (Å): Pt-N1, 1.956(1); Pt-N3, 2.046(1); Pt-Cl1, 2.274(1); Pt-Cl2, 2.294(1); N1-C2, 1.291(1); N3-C3, 1.497(1). Angles (°): N1-Pt-N3, 80.8(1); N3-Pt-Cl1, 90.7(1); Cl1-Pt-Cl2, 91.6(1); Cl2-Pt-N1, 96.8(1); C2-N1-Pt, 119.9(1); C3-N3-Pt, 112.2(1); C2-C3-N3, 110.5(1).

Figure 4: pH dependent ligand **3** enolization ratio (keto /enol) using RP-HPLC Partisil C-18 ODS.

Table 1. Biological properties of the reference (Stattic) and of the oxadiazole derivatives.

Figure 5. Body weight changes. The body weight changes of LLC-bearing C57BL mice treated with vehicle or tested compounds. Body weight was measured at day 1 and every two days from day 7 and was taken as a parameter of systemic toxicity. The error bars indicate the SD.

Table 2. *In vivo* antitumor activity toward LLC.

Figure 6. Cytotoxic effects of **Pt-3** complex and cisplatin on DLD-1, HCT-116 and MCF-7 cell lines. Cells were seeded at the density of 40,000/well in a 48 well tray. The day after the medium was replaced with one containing 10% FCS and the reported concentrations of **Pt-3** and cisplatin. After 48 h the cell viability

was estimated by MTT assay. Each bar represents the mean ± SD of three determinations. **Pt-3** and cisplatin *vs* control *P < 0.05;**P < 0.01; ***P < 0.001.

Figure 7. DNA and total intracellular concentrations of ^{195}Pt in HCT-116 cell line incubated with **Pt-3** and cisplatin. Cells were seeded (250,000/35 mm petri dish) and incubated with McCoy's supplemented with 10% FCS; 24 h later the medium was replaced with one containing 10% FCS and indicated concentrations of **Pt-3** or cisplatin. After 3 h, the nuclear DNA and total cell homogenates were prepared and ^{195}Pt concentrations determined by ICPMS and normalized with total DNA (A) and protein contents (B).

Figure 8. Effect of **Pt-3** on p53 expression in HCT-116 cell line. Cells were seeded (250,000/35 mm petri dish) and incubated with McCoy's supplemented with 10% FCS; 24 h later the medium was replaced with one containing 10% FCS and the reported concentrations of **Pt-3** and cisplatin. The incubation was continued for a further 24 h at 37°C and Western blot analysis was performed from total cell lysates. *α*-tubulin antibody was utilized as loading control.

Figure 9. Effect of ligand **3** · **HCl** and **Pt-3** on STAT3 activity in cultured cells. (**A** and **B**) HCT-116 cells were seeded and incubated with McCoy's supplemented with 10% FCS; 24 h later the medium was replaced with one containing 10% FCS and the reported concentrations of **3** · **HCl** and **Pt-3**. The incubation was continued for a further 24 h at 37°C and Western blot analysis (**A**) were performed from total cell lysates. The ratio of phosphoSTAT3/STAT3 signals are shown in the histogram plot. (**B**) Luciferase reporter assay for STAT3 transcriptional activity was performed in HeLa stable cells pre-incubated for 2 h with reported concentrations of **3** · **HCl** and **Pt-3**. The luciferase activity was the stimulated by adding Oncostatin M for 4 h. ** p < 0.01; *** p < 0.001 *vs* control (Cnt).

Figure 10. AlexaFluor488-maleimide labeled STAT3 competition assay: a pre-treatment with test compounds assay (**A**) and post-treatment with test compound one (**B**)